Microcoil MRI of plants and algae at ultra-high field : an exploration of metabolic imaging

Schadewijk, R. van

3 MR MICROSCOPY USING MICROCOILS AT 22 T: COIL CALIBRATION AND USAGE

Demonstrated on *Medicago truncatula* roots.

3.1 ABSTRACT

This chapter describes a method that was developed to calibrate microcoils designed for ultra-high field (22.3T), high-resolution magnetic resonance imaging (MRI). Microcoils increase sensitivity by matching the size of the RF resonator to the size of the sample of interest, thereby allowing higher image resolutions. Due to the relatively simple design, solenoidal microcoils can be custom made and adapted to the sample requirements. Systematically, I explain how to calibrate new or home-built microcoils, using a reference solution. The calibration steps include 1. pulse power determination using a nutation curve 2. Estimation of RF-field homogeneity and 3. calculating a volume normalised Signal-to-Noise Ratio (SNR) using standard pulse sequences. Important steps in sample preparation for small biological samples are discussed, as well as and possible mitigating factors such as magnetic susceptibility differences. The applications of an optimised solenoid coil are demonstrated by high-resolution ($13 \times 13 \times 13$ μm^3, 2.2 fL) 3D imaging of a *Medicago truncatula* root sample.

This chapter will be published as a video protocol:

van Schadewijk, R., Krug, J.R., Webb, A., van As, H., Velders, A.H., de Groot, H.J.M., Alia, A. (2019). Ultra-High Field Magnetic Resonance Microscopy using Microcoils: coil performance calibration and usage demonstrated on *Medicago truncatula* roots. (Manuscript submitted)

3.2 INTRODUCTION

Magnetic Resonance Imaging is a versatile tool to non-invasively image a wide variety of biological specimens, ranging from humans to single cells (Aguayo *et al.*, 1986; Ciobanu and Pennington, 2004; Radecki *et al.*, 2014). While MRI-scanners for medical imaging applications typically use magnets with a field strength of 1.5 T to 3 T, single-cell applications are imaged at much higher field strengths (Ciobanu and Pennington, 2004; Radecki *et al.*, 2014; Lee *et al.*, 2016). The study of specimens at resolutions below a hundred micrometres is referred to as Magnetic Resonance Microscopy (MRM) (Callaghan, 1993). However, MRM suffers from a low Signal-to-Noise Ratio (SNR) compared to other available microscopy or imaging techniques (*e.g.*, optical microscopy or CT). To optimise the SNR, several approaches can be pursued (Glover and Mansfield, 2002). One approach is to use a higher magnetic field strength, while a complementary approach is to optimise the signal detector for individual samples. For the latter, the dimensions of the detector should be adjusted to match the dimensions of the sample of interest. For small samples (≈0.5-2 mm in diameter), *e.g.*, root tissues, microcoils are useful as the SNR is inversely proportional to the coil diameter (T L Peck, Magin and Lauterbur, 1995; Glover and Mansfield, 2002). Resolutions as high as 7.8 x 7.8 x 15 μm^3 have been attained on animal cells using dedicated microcoils (Lee *et al.*, 2015). A variety of microcoil types exist, with planar and solenoid coils most commonly used depending on application and tissue geometry (Fratila and Velders, 2011). For example, a method designed specifically for imaging perfused tissue has been described for planar microcoils (Flint *et al.*, 2017). In this chapter, the characteristics of the solenoid coil are described as well as a protocol to prepare samples for microcoil MRI and the required steps to calibrate solenoid microcoils (Fig. 3.1A).

The solenoid coil consists of a conducting wire looped, like a corkscrew, around a capillary holding the sample. Used in combination with the specific MR system (Materials and Methods), microcoils can be constructed using only enamelled copper wire, an assortment of capacitors, and a suitable base for soldering the components (Fig 3.1B). The major advantages are the simplicity and low cost, combined with good performance characteristics in terms of SNR per unit volume and B_1 field homogeneity. The ease of construction enables fast iteration of coil designs and geometries. The specific requirements of solenoid microcoil design and probehead characterisation, *i.e.* the theory of electronics, workbench measurements and spectrometer measurements for a variety of coil geometries, have been described extensively elsewhere (T L Peck, Magin and Lauterbur, 1995; Haase *et al.*, 2000; Minard and Wind, 2001a, 2001b; Vegh *et al.*, 2012).

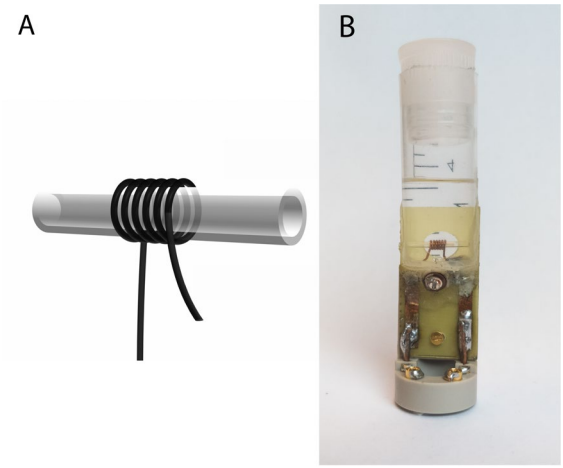

Fig. 3.1 A solenoid microcoil. (A) The solenoid coil design consists of wire looped helically, typically wrapped around a capillary. The geometry of the wire, such as its thickness, diameter, number of windings and wire spacing influence the coil characteristics. **(B)** A home-built solenoid microcoil with a reservoir for susceptibility matching fluid (Fomblin). It consists of a 0.4 mm thick coated copper wire wound six times around capillary with an outer diameter of 1500 µm. The coil is submerged in a reservoir which is made from a syringe. Sample capillaries up to an outer diameter of 1000 µm can be inserted. Two capacitors are used, a 1.5 pF capacitor in series with the inductor and a second variable 1.5-6 pF capacitor is placed in parallel to the inductor. All components are soldered to a fibreglass board (yellow). It is mounted on a commercial holder (grey polymer) that is modified to support the reservoir.

Basic experimental MR parameters are highly dependent on the hardware of the system used, including gradient system, field strength, and console. Several parameters can be used to describe the system performance, of which 90° pulse power, B_1-homogeneity and SNR per unit volume (SNR/mm^3), are the most practically relevant.). To this end, a standardised spin echo measurement using a phantom has been adapted to microcoils (Oerther, 2012). SNR/mm^3 is useful to compare the performance of different coils on the same system. While hardware differences across systems may exist, the uniform application of a benchmarking protocol also facilitates the comparison of system performance.

This protocol focuses on calibration and sample preparation. The stepwise characterisation of the performance of solenoid microcoils is shown: 1. calibrating the 90° pulse length and power 2. Assessing the RF-field homogeneity and 3. calculating SNR per unit volume (SNR/mm^3). A standardised spin echo measurement using a phantom is described to facilitate comparison of coil designs, which allows for optimisation of distinct applications. Phantom and biological specimen sample preparation, specific for microcoils, are described. The protocol may be implemented on any suitable narrow-bore (≤ 60 mm) vertical spectrometer equipped with a microimaging system. For other systems, it can serve as a guideline and can be used with some adjustments.

Biological specimen preparation for MRI measurements is usually not very extensive since the specimen is imaged as intact as possible. However, air spaces in biological tissue can cause image artefacts due to differences in magnetic susceptibility (Callaghan, 2007). The effect increases with increasing magnetic field strength (Donker *et al.*, 1997). Thus, air spaces should be avoided at high-field strengths, and this might require the immersion of the sample in a fluid to avoid air around the tissue and the removal of air spaces within the tissue structures. Specifically, when microcoils are employed, excision of the desired sample tissue might be required, followed by submerging it in a suitable fluid. This is followed by insertion of the sample into a pre-cut capillary, and finally sealing the capillary with capillary wax. Using wax as a sealant instead of glue, flame-sealing or alternatives, means that the sample may be easily extracted. This procedure is demonstrated on the root of *Medicago truncatula* a small leguminous plant. The advantage of co-registration of MRI data with optical microscopy is highlighted since the sample is not destroyed during the MRI measurement.

The presented protocol is suitable for high spatial resolution *in situ* measurements, and more elaborate designs could allow for imaging *in vivo* samples, where challenges related to life support systems would need to be addressed.

3.3 PROTOCOL

This protocol describes the necessary procedures to evaluate coil characteristics of a 1.5 mm inner diameter (ID) solenoid coil (Fig. 3.1B). The coil used to demonstrate the protocol is housed in a susceptibility-matched reservoir, but the protocol is equally applicable to unmatched coils. The protocol may be adapted to other sizes and different spectrometer setups.

A solenoid coil can be built by keeping in mind design rules for the desired dimensions according to the guidelines described elsewhere (Timothy L. Peck, Magin and Lauterbur, 1995; Webb, 2013). In this specific case, a coil was used with an inner diameter of 1.5 mm, made from 0.4 mm enamelled copper wire looped around a capillary of 1.5 mm outer diameter. This solenoid is held on a base plate on which a circuit is made, a tuning capacitor (2.5 pF), a matching capacitor (1.5-6 pF) as well as with copper connecting wires. The exact values of the capacitors are determined by the desired resonance frequency.

The susceptibility-matched design of the coil includes a reservoir with perfluorinated liquid to reduce susceptibility mismatches, arising from the copper coil being in close proximity to the sample (Olson *et al.*, 1995). A reservoir was made out of a plastic syringe to enclose the coil and filled with fomblin. As the perfluorinated liquid needs to enclose the coil, the available diameter for a sample is reduced to an outer diameter of 1 mm. For ease of sample changing, the sample was prepared in a capillary with an outer diameter of 1 mm and an inner diameter of 700 µm. The necessary tools for sample preparation are shown in Fig 3.2A.

The coil can be mounted on a holder which fits the Bruker Micro5 probe. In this case, a modified support insert was used, equipped with the necessary connections to connect to the ^{1}H channel of the Micro5 probe.

3.3.1. REFERENCE SAMPLE PREPARATION

3.3.1.1. To prepare 100 ml of the sensitivity reference solution, dissolve 156.4 mg of $CuSO_4 \cdot 5\ H_2O$ into 80 mL of D2O contained in a 100 mL GL45 flask. Manually stir until solids are completely dissolved.

3.3.1.2. Adjust volume to 100 ml using de-ionised water for a final concentration of 1 g L^{-1} $CuSO_4$ (anhydrous).

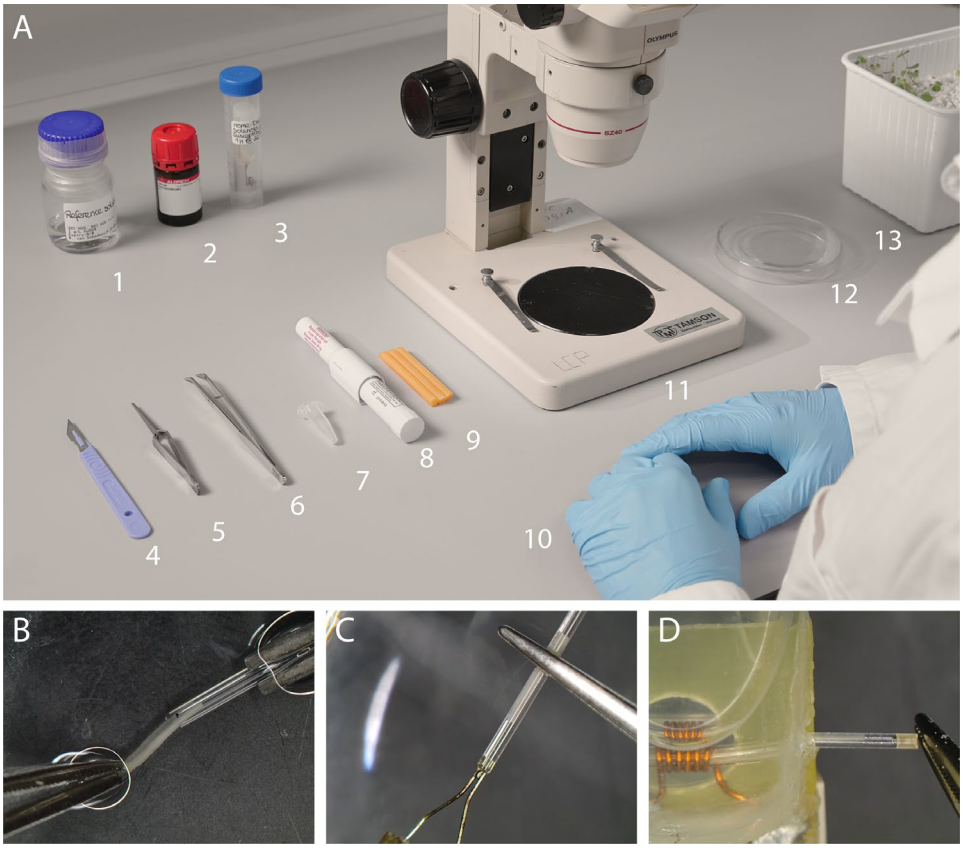

Fig. 3.2 Sample preparation under a stereomicroscope. (A) Items needed for the preparation of microcoils. From left to right: 1. $CuSO_4$ reference solution, 2. perfluorodecalin, 3. microcoil, 4. scalpel, 5. positive tension tweezers, 6. tweezers, 7. capillaries outer diameter = 1000 µm, 8. wax pen, 9. capillary wax, 10. nitrile gloves, 11. stereomicroscope, 12. watch glass with petri dish cover, 13. plant material in growth substrate. Not shown: 2 mL syringe with ø 0.8 × 40 mm needle and fine tissue paper. **(B)** Close up of sample insertion into a capillary using tweezers, while both are kept submerged. **(C)** Sealing of the capillary using molten wax. **(D)** Insertion of the prepared capillary into the microcoil.

NOTE: The reference sample should be sealed to prevent changing the ratio of H_2O: D_2O.

3.3.2. SAMPLE PREPARATION

3.3.2.1. If preparing a reference sample, add 1 ml $CuSO_4$ solution to a watch dish under a stereomicroscope.

3.3.2.2. If preparing a biological sample, place 1 ml of perfluorodecalin (PFD) inside a watch glass under a stereomicroscope. PFD will infiltrate a biological specimen without entering the intact cells and thereby reduce the number of air cavities. Immediately cover the watch glass with a petri dish lid to prevent evaporative loss, until the PFD is needed. NOTE: PFD is highly volatile and a potent long-term greenhouse gas (Tsai, 2011). When its oxygen-dissolving properties and its low viscosity are not required, it may be substituted with Fomblin, a perfluoroether which also gives no observable ^1H signal, but which does not evaporate as quickly (Olson *et al.*, 1995).

3.3.2.3. Capillaries of suitable outer diameter need to be cut to size, to fit inside the diameter of the microcoil holder (18 mm) and allow for repositioning (Fig. 3.1B). Use a ceramic cutter to make an incision every 10-12 mm and break carefully on the incision point.

3.3.2.4. If preparing a reference sample, use tweezers and the stereo microscope, to bring a pre-cut capillary in contact with the surface of the $CuSO_4$ solution inside the watch glass, allowing capillary action to fill the capillary.

3.3.2.5. If preparing a biological sample, use tweezers and a stereo microscope, to bring a pre-cut capillary in contact with the surface of the PFD inside the watch glass, allowing capillary action to fill the capillary fully. Release the capillary into the watch glass so that it becomes fully submerged.

3.3.2.5.1. Next, carefully extract a whole root system from its soil or soil replacement. Clean the root sample meticulously. Photograph if needed for future reference. Select and excise a root section using a scalpel.

To reduce the presence of air pockets within biological samples:

3.3.2.6. Place the sample into a 1.5ml Eppendorf tube containing a suitable buffer solution. Leave the tube cap off, then apply parafilm to seal the opening of the tube. Then, punch holes with a sharp tool to allow for ventilation of the tube.

3.3.2.7. Place the sample tube in a vacuum chamber, seal the chamber, connect a vacuum pump to the chamber and apply vacuum for 30 minutes. Air bubbles may be seen escaping the sample.

3.3.2.8. Using tweezers and stereomicroscope, submerge the sample in the infiltration medium prepared previously. Wash the sample of potential debris.

3.3.2.9. Next, insert the sample into the capillary using tweezers, while both capillary

and sample are fully submerged in order to avoid inclusion of air bubbles. A smaller capillary or syringe may serve as a pushing rod (Fig. 3.2B).

3.3.2.10. Take the sample capillary from the watch glass, using tweezers. In the case of PFD, cover the petri-dish lid.

3.3.2.11. Remove circa 1 mm of liquid from both ends of the capillary using fine tissue paper.

3.3.2.12. Melt a small volume of capillary wax using a wax pen. Apply wax on either side while taking care to eliminate any possible air pockets with the capillary (Fig. 3.2C). When the wax has hardened, it will become opaque.

NOTE: Avoid overheating wax or capillary as this may cause explosive boil off as well as cavitation pockets when the finished sample cools.

3.3.2.13. Remove excess wax from the exterior of the capillary with a scalpel and wipe clean with fine tissue paper.

3.3.3. MOUNTING SAMPLE

3.3.3.1. Place a microcoil underneath the stereo microscope and insert the sample using tweezers while immobilising the microcoil (Fig. 3.2D).

3.3.3.2. Position the sample in the centre of the coil by sliding the capillary inside the solenoid coil.

3.3.3.3. Optionally, apply scotch tape to fix the position of the capillary.

3.3.3.4. Inspect the capillary to ensure no air bubbles are visible inside the solenoid coil, to avoid MR signal destruction caused by susceptibility differences.

3.3.3.5. Place the microcoil on the socket of the probe base (Fig. 3.3A & B).

3.3.3.6. Carefully slide the gradient coils over the microcoil while matching the water-cooling connectors of the gradient to that of the probe base (Fig. 3.3C). (Note: This step applies for a Micro5 probe only. In the case of a Micro2.5 or a Biospect system, the gradients are on a separate socket than the coil)

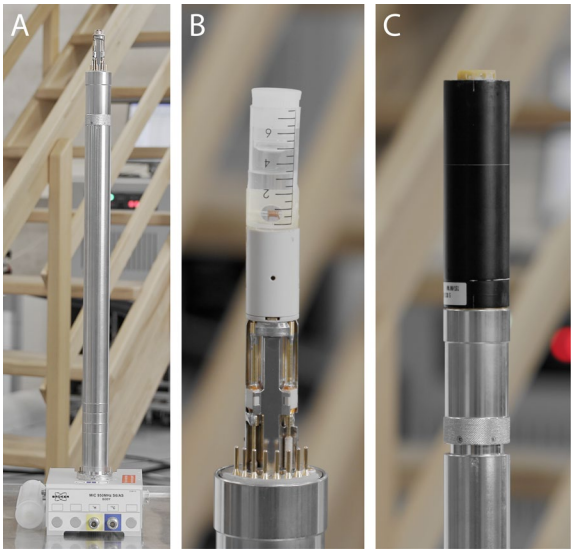

Fig. 3.3 The components of a micro-imaging probe. (A) Micro5 probe base, containing all necessary connections for water cooling, heating, temperature sensors, gradient power, RF (co-axial connector visible) and optionally probe identification (PICS). Underneath the probe base are knobs that allow for adjusting the variable tuning and matching capacitors, as well as retaining screws to hold the probe in place inside the spectrometer. **(B)** The home-built microcoil mounting atop the probe-base. Note the variable capacitors (white ceramic) mounted on the probe-base that allow for tuning and matching. **(C)** Integrated 3-axial gradient mounted on the probe base with water-cooling receptacles and gold-plated contacts for grounding the gradient.

3.3.4. DETERMINING COIL CHARACTERISTICS

If the coil is tested for the first time, it is recommend to use the reference sample solution to create a homogeneous sample, which is useful for power calibration and B_1 homogeneity tests. Also, potential susceptibility problems due to the coil wires may be tested easily with this reference sample.

3.3.4.1. To test if the coil resonates at the desired resonance frequency, the probe base can be connected to a network analyser. An S_{11} test can be performed to test the frequency range achieved by tuning and for Q-factor measurements as described in Haase *et al*. (Haase *et al.*, 2000).

3.3.4.2. Insert the probe into the magnet and connect all cables.

3.3.4.3. Set desired water-cooling temperature (recommended 298 K) for the water cooling unit (BCU20).

3.3.4.4. Set the target temperature (298 K) and the target gas flow (300 L h^{-1}). The gas flow might be different for a different coil design or sample volume. This applies only to systems with a temperature control system.

NOTE: The next steps are only necessary when test novel (home-built) coils.

3.3.4.5. Connect the probe using a 50 Ω co-axial cable to a network analyser with a suitably wide sweep width (400 MHz), centred on the intended resonance frequency.

3.3.4.6. Observe the resonant modes by adjusting the matching and tuning capacitors of the probe base.

3.3.4.7. Tune and match the resonant mode to the desired frequency.

3.3.4.8. Optionally, determine the coil quality factor (Q-factor) on a network analyser. One method to obtain the quality factor is to use a coupling network and dividing the centre frequency by the width of the resonance peak at -3 dB (*i.e.*, $Q = 2 * f_c/(f_1 - f_2)$) (Haase *et al.*, 2000). Some network analysers have Q-factor determination built-in.

3.3.4.9. Initiate a wobble curve and adjust the tuning and matching as necessary. It is recommended to set any tuning and matching capacitors to the midpoint of their range for new coils. Therefore, using a high spectral sweep width is recommended. In some cases, it might be more convenient to tune and match the coil outside the magnet on a network analyser.

3.3.4.10. Select a shim file for the largest volume coil of the imaging probe if it is available. If starting from a coil which has been used previously, use an available shim file. If both options are not available, start with all shim values set to 0.

3.3.4.11. Select correct coil configuration if it is available in the imaging software (*i.e.*, ParaVision). Else, create a new coil configuration matching the specifications of the coil, *e.g.*, single tuned or double tuned, according to the manual of your system. Estimations for the safe limits for this solenoid microcoil used in this research with 1.5 mm inner diameter in size is 1 ms at 1W peak power and 1 mW continuous power.

CAUTION: The small capacitors (typically 1 mm in size) needed for microcoils are highly sensitive and easily damaged by high voltages. Automated pulse power determination might not function with non-standard coils, and too high powers could cause damage to the coil or other parts of the spectrometer. Therefore, manual adjustments are recommended.

3.3.4.12. A nutation curve should be recorded for a new coil to obtain an indication of the correct rf-power for the coil (Fig. 3.4). Using an FID-experiment in the absence of gradient encoding, the RF-pulse length is varied systematically while the pulse power is kept constant. The ideal pulse length is the pulse length where the signal intensity reaches the maximum. If testing a new coil, use a 10 µs pulse with a very low power first and start increasing the pulse power gradually. In case the power is much higher than expected for the

combination of coil characteristics and spectrometer, this is already an indication that the wrong resonant mode has been selected. For a coil with a homogeneous B_1-field, like a solenoid coil, the 180° pulse can also be determined where the signal intensity decreases to zero (Keifer, 1999).

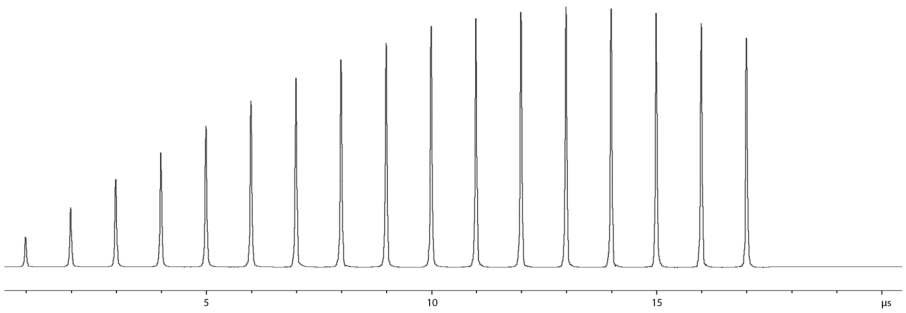

Fig. 3.4 Nutation curve. A nutation curve is acquired to determine the reference pulse power. The reference pulse power (90° pulse) is defined as the combination of power and pulse length needed to generate a B_1 field that flips all available magnetisation in the z-direction to the transverse plane. A series of a pulse is recorded in the absence of gradient encoding. With each pulse, either pulse length or pulse power is incremented. Here the pulse power is set to 0.6 W, while the pulse length is incremented by 1 µs each time. The maximum signal intensity indicates the 90° pulse, around 12-13 µs. The 180° pulse may also be determined in this way using the minimum intensity.

3.3.4.13. Set the determined 90° pulse power into the adjustment card of the created study (In ParaVision, the reference power adjustment card may be used to enter the hard pulse power).

3.3.4.14. Use a Localiser scan with 3 slices, one slice in each of the three primary axes, to locate the position of the coil within the magnet. Starting with a large field-of-view is recommended. If the sample is exactly in the centre of the gradient system, the Localizer scan will show the sample. If the coil or sample is not centred in the image slices or missing, the localiser scan might need to be adjusted.

3.3.4.15. A complementary way to find the correct 90° pulse is based on image evaluation: Once an approximate pulse power is found, one could adjust the pulse powers gradually to check the image for B_1-field homogeneity. For some coils, the 90° pulse power determined using the nutation curve could be overestimated, which leads to over-tipping in the homogeneous region of the B_1 field. The pulse reference pulse may then be reduced, and the new images can be checked against the previous images (Fig. 3.5).

3.3.4.16. Manually shim the magnetic field based on the FID signal. A recommended order for initial shimming is Z-Z^2-Z-X-Y-Z-Z^2-Z-XY-XZ-YZ-Z. In the case of a solenoid, the main symmetry-axis is in the XY-plane. Therefore, shims in different directions might be more sensitive for this coil configuration. Higher

order shims have little effect and may be ignored.

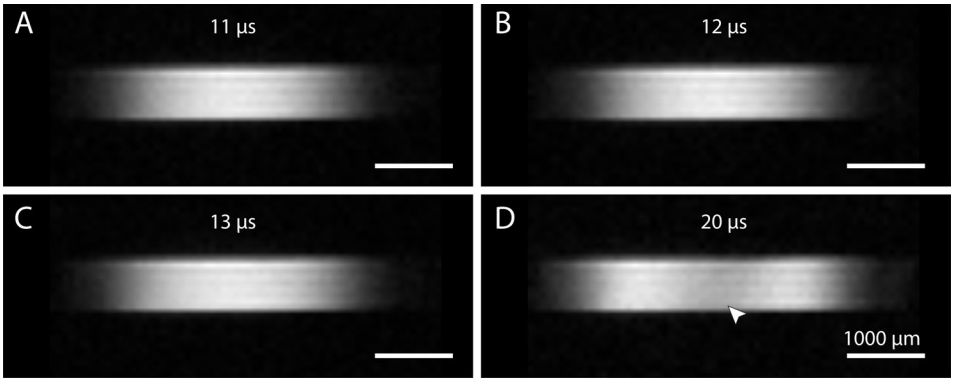

Fig. 3.5 Visual determination of 90° pulse power Once an approximate reference pulse power has been found using a nutation curve, it may be checked visually by varying the pulse length. Depending on the coil, the B_1 field may be more or less sensitive to changes. **(A)** 11 µs pulse length. **(B)**12 µs pulse length, optimal for this coil. **(C)** 13 µs pulse length. **(D)** 20 µs pulse length. If the pulse power is set too high, over-tipping may occur, thereby reducing image intensity in the centre of the coil (arrowhead). The increased B_1 field also increases the range of the coil, as can be observed in the width of the image.

3.3.4.17. Next, a volume-normalised SNR must be calculated to allow for comparison of coil characteristics across different systems, adapted from the manufacturer's protocol (Oerther, 2012). A spin echo sequence is used with the following parameters: FOV 6 mm x 6mm TR 1000 ms, TE 7 ms, Matrix 256 x 256 and Slice thickness = 0.5 mm. Adjust the slice thickness until the receiver gain is unitary. Next, adjust the number of slices so that slices extend beyond the region of B_1-field homogeneity. Record the images without signal averaging if possible.

3.3.4.18. The volume normalised SNR (SNR/mm^3) can be determined in two steps. First, the Voxel volume (V_{voxel}) is calculated (Eq. 3.1):

$$V_{\text{voxel}} = D_x \times D_y \times D_{\text{slice}} \tag{3.1}$$

Then, by selecting regions of interest, determine the signal intensity (μ) and standard deviation (σ) of the sample (*i.e.*, the signal) and a region outside the sample (*i.e.*, the noise). Either the spectrometer control software or general-purpose image processing software may be used for these calculations. The values may then be used to calculate a volume normalised SNR (Eq. 3.2):

$$SNR_{\text{v}} = \frac{\mu_{\text{ROI}} - \mu_{\text{noise}}}{\sigma_{\text{noise}} \times V_{\text{voxel}}} \tag{3.2}$$

When comparing the SNR of coils at different magnetic field strengths, the relaxation properties would need to be taken into account(Vlaardingerbroek and Boer, 2013).

NOTE: The units for D_x, D_y and D_{slice} are in mm. This calculation can likewise be performed for a series of slices.

3.3.4.19. Check for susceptibility problems due to magnetic field inhomogeneities: load and run a multiple gradient-echo (MGE) sequence (Fig. 3.6). Magnetic field inhomogeneities due to susceptibility differences are visible in the images with higher echo times as the gradient echo does not refocus spins which dephase due to static field inhomogeneities. This way inhomogeneities in the sample may be visualised (due to, *e.g.*, air spaces in the sample), as well as B_0 field inhomogeneities introduced by the coil material. The following parameters are suggested, to be adjusted depending on the specifications of the spectrometer and coil used: repetition time 200 ms, echo time 3.5 ms with 48 echoes spaced 3.5 ms apart, flip angle 30 degrees. Matrix size 128 × 128.

NOTE: If multiple resonant modes were observed in the resonance (wobble) curve, repeat the above steps for each resonant mode to determine the most sensitive one.

3.3.5. HIGH-RESOLUTION IMAGING

3.3.5.1. Run a 3D-FLASH experiment with the following suggested parameters: Repetition time 70 ms, echo time 2.5 ms, matrix size of 128 × 64 × 64, field of view 1.6 × 0.8 × 0.8 mm, and receiver bandwidth 50 kHz. Adjust the FOV, if necessary, to cover the whole object in both phase encoding directions, thereby avoiding aliasing.

3.3.6. RECOVERING SAMPLES FOR FURTHER STUDY OR STORAGE

3.3.6.1. Remove the sample capillary from the microcoil.

3.3.6.2. Using tweezers, remove the wax plugs under a stereomicroscope.

3.3.6.3. A syringe may be used to wash the sample out of the capillary with a solution of choice. Alternatively, a glass pusher rod may be used to eject the sample.

3.3.6.4. To prevent dehydration of the sample, store in a suitable medium for storage.

3.4 REPRESENTATIVE RESULTS

3.4.1 COIL CHARACTERISATION

Upon successful tuning and matching of a coil, its performance may be characterised by the coil Q-factor, 90° reference pulse, and SNR/mm^3. For the 1,5 mm ID susceptibility-matched solenoid coil demonstrated here, the Q-factor(unloaded) was 244, compared to 561 for a 5 mm birdcage coil.

The reference 90° pulse was 10-12 µs at a power level of 0.6W; *cf.* a 5mm birdcage coil used in the same spectrometer was 5 µs at 45 W. See also Fig. 3.5. The most relevant to image quality, however, is the SNR_v for the microcoil. For the coil used here, filling in Eq. 3.2 results in the following:

$$SNR_v = \frac{2.3 \cdot 10^{1} - 3.4 \cdot 10^{-1}}{1.8 \cdot 10^{-1} \times 2.75 \cdot 10^{-4}\ mm^3} = 4.6 \cdot 10^{5}\ mm^{-3} \tag{3.3}$$

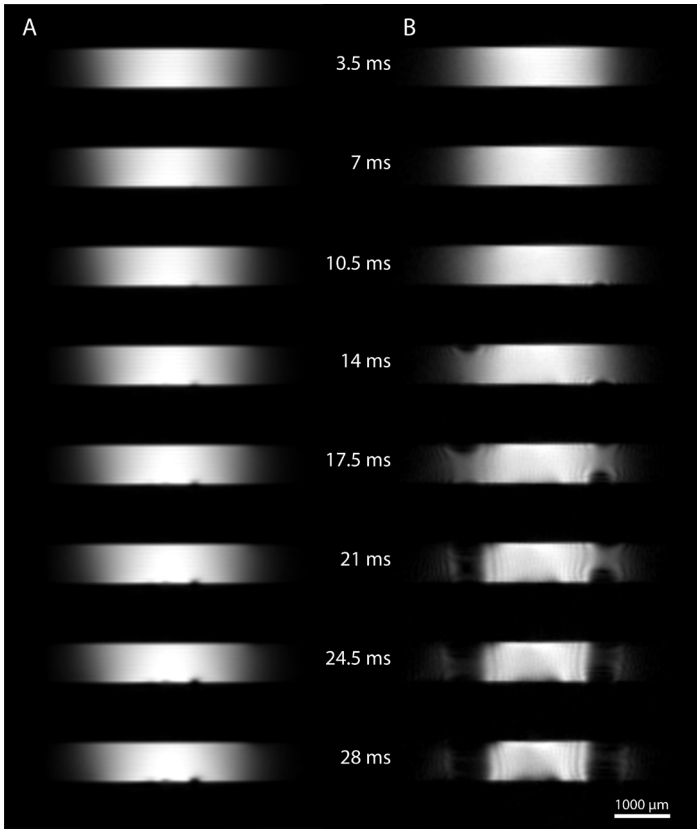

Fig. 3.6 RF homogeneity evaluated by gradient echo imaging. A Multiple Gradient Echo (MGE) sequence is used to evaluate RF (B_1 -Field) homogeneity using a series of gradient echoes. Basic parameters were: repetition time 200 ms, echo time 3.5 ms with number of echoes 48, echo spacing 3.5 ms, 64 averages, acquisition time 27 m 18 s, flip angle 30 degrees. Field of view was 5 × 5 mm, matrix 128 × 128, resolution 39 × 39 × 200 µm^3. **(A)** Susceptibility-matched coil. The susceptibility matching fluid (Fomblin) surrounding the RF coil reduces susceptibility effects due to the coil wire. Small air bubbles cause loss of signal as the echo time increases. **(B)** A coil (not susceptibility matched) with equal coil diameter. At longer echo times increasing artefacts caused by B_0 field inhomogeneity are observed.

3.4.2 EFFECT OF SUSCEPTIBILITY MATCHING

At ultra-high field strengths, sample and coil susceptibility become a dominant factor for image quality as seen in Fig. 3.6A and B. Compared to a coil lacking a susceptibility matching fluid reservoir, the signal is retained longer and more homogeneously in a reference sample. However, due to the susceptibility reservoir, the maximum sample dimensions decrease with respect to the coil without the reservoir.

3.4.3 HIGH-RESOLUTION IMAGING

A high resolution of 13 × 13 × 13 μm^3 of a *Medicago truncatula* root specimen was attained in 20 hours and 23 minutes (Fig. 3.7). Starting from the surface of the root, the root cortex is seen, along with some residual water on the outside of the root. Furthermore, the xylem is observed as a dark band enclosing the phloem. Some air pockets are observed as dark spots with near-complete signal loss.

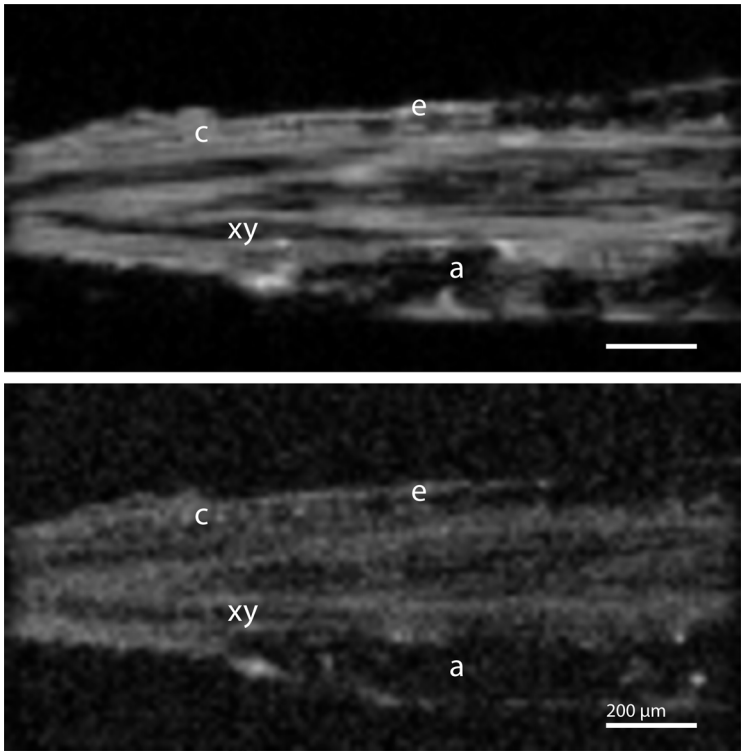

Fig. 3.7 3D imaging of a *Mediago truncatula* root section. **(A)** FLASH image. Several features of the root section can be distinguished, including the epidermis (e), cortex (c) and xylem (xy). Air pockets (a) in the root cause complete signal loss. Basic parameters were as follows: Repetition time 70 ms, echo time 2.5 ms, 256 averages, acquisition time 20 h 23 m. Resolution 13 × 13 × 13 μm^3. Matrix size was 128 × 64 × 64 and field of view 1.6 × 0.8 × 0.8 mm. Receiver bandwidth 50 kHz. **(B)** MSME image. Basic parameters were as follows: Repetition time 500 ms, echo time 5.2 ms, 28 averages, acquisition time 15 h 55 m. Resolution 13 × 13 × 13 μm^3. Matrix size was 128 × 64 × 64 and field of view 1.6 × 0.8 × 0.8 mm. Receiver bandwidth 70 kHz.

3.5 DISCUSSION

Even for simple circuit designs, multiple resonant modes can be present, especially near capacitors close to the solenoid coil. These alternate modes represent a pathway for RF transmission loss and reduce the overall sensitivity of the coil. Identifying the primary resonant mode is therefore important but can be affected strongly by the properties of the probe to which it is mated. Hence, coils have to be developed in conjunction with the probe base which contains adjustable tuning and matching capacitors.

As microcoils are ideally very close to the sample, the magnetic susceptibility differences between the medium and the wire can cause additional signal loss. For this reason, we presented a susceptibility-matched coil, by submerging the wire in fluorinert liquid (Fomblin or FC-43). An alternative approach for constructing a susceptibility matched coil is to use susceptibility- matched wire (Kc *et al.*, 2010). Furthermore, only susceptibility issues due to the coil are addressed with this approach. Susceptibility mismatches inside the sample (*e.g.*, due to air spaces) remain challenging.

Air pockets or bubbles pose an experimental challenge that causes extensive signal loss, caused by susceptibility differences at the interface of the air and the fluid or specimen (Callaghan, 2007) (Fig. 3.5A). An important aspect for successful sample preparation is the submersion of both sample and capillary. However, even small bubbles can cause signal losses, especially for gradient echo type sequences. Mobile air bubbles can migrate through the capillary until they are in contact with the sample. Some of these effects can be alleviated by slightly tilting the capillary so that on end is higher than the other. Tilting ensures potential air bubbles are held in place at the higher end, without disturbing the sample.

For the air spaces inside the sample, PFD was used to fill up the intercellular air spaces (Littlejohn *et al.*, 2010) while not penetrating the cell membranes. However, even with this approach, we were not able to remove all air spaces. Additionally, this approach means that we need an additional agent, which is usually not preferred due to the desire to study a system as non- invasive as possible.

The cylindrical shape of capillaries means that perfusion setups should be viable, especially for tissues vulnerable to decay such as biopsies or studying processes in living root material. Two steps could realise a perfusion setup. First, by connecting and a medium feed tube and drain tube at either side of the capillary would be sufficient to create a chemostat. Second, the addition of an indentation in the sample capillary could hold the sample in place against the direction of flow. This is analogous to a protocol published for planar microcoils (Flint *et al.*, 2017).

The non-invasive nature of MR imaging, combined with the inert liquid used in this protocol (PFD or Fomblin), means that after completion of experiments samples may be removed from their capillaries for further study. Combinations include optical or electron microscopy and other destructive imaging techniques.

We have demonstrated a method for imaging plant material using dedicated microcoils on an ultra-high field NMR spectrometer. Relatively large sample volumes can be studied at high resolution with RF homogeneity. Adapting microcoil design to samples is facilitated by an efficient method to determine coil performance characteristics. The solenoid coil approach may also be readily applied to other samples than plants, including animal tissue.

3.6 ACKNOWLEDGEMENTS

Experiments at the 950MHz instrument were supported by uNMR-NL, an NWO-funded National Roadmap Large-Scale Facility of the Netherlands (project 184.032.207). R.S. was supported by the BioSolarCells consortium project U2.3. J.R.K. was supported by the Netherlands' Magnetic Resonance Research School (NMARRS) graduate school [022.005.029]. Klaartje Houben, Marie Renault and Johan van der Zwan are thanked for technical support at the uNMR-NL facility. Further thanks go out to Volker Lehmann, Henny Janssen and Pieter de Waard for technical help. Lastly, we express our gratitude to Frank Vergeldt, John Philippi and Karthick B. Sai Sankar Gupta for their advice.

3.7 REFERENCES

Aguayo, J. B. *et al.* (1986) 'Nuclear magnetic resonance imaging of a single cell.', *Nature*, 322, pp. 190–1. doi: 10.1038/322190a0.

Callaghan, P. T. (1993) *Principles of nuclear magnetic resonance microscopy*. Oxford University Press on Demand.

Callaghan, P. T. (2007) 'Susceptibility and Diffusion Effects in NMR Microscopy', *Encyclopedia of Magnetic Resonance*. doi: 10.1002/9780470034590.emrstm0549.

Ciobanu, L. and Pennington, C. H. (2004) '3D micron-scale MRI of single biological cells', *Solid State Nuclear Magnetic Resonance*, 25(1–3), pp. 138–141. doi: 10.1016/j.ssnmr.2003.03.008.

Donker, H. C. W. *et al.* (1997) 'Quantitative 1H-NMR imaging of water in white button mushrooms (Agaricus bisporus)', *Magnetic Resonance Imaging*, 15(1), pp. 113–121. doi: 10.1016/S0730-725X(96)00328-1.

Flint, J. J. *et al.* (2017) 'Metabolic support of excised, living brain tissues during magnetic resonance microscopy acquisition', *Journal of Visualized Experiments*, 2017(128), pp. 1–10. doi: 10.3791/56282.

Fratila, R. M. and Velders, A. H. (2011) 'Small-volume nuclear magnetic resonance spectroscopy.', *Annual review of analytical chemistry (Palo Alto, Calif.)*, 4, pp. 227–49. doi: 10.1146/annurev-anchem-061010-114024.

Glover, P. and Mansfield, S. P. (2002) 'Limits to magnetic resonance microscopy', *Reports on Progress in Physics*, 65(10), pp. 1489–1511. doi: 10.1088/0034-4885/65/10/203.

Haase, A. *et al.* (2000) 'NMR probeheads for in vivo applications', *Concepts in Magnetic Resonance*, 12, pp. 361–388. doi: 10.1002/1099-0534(2000)12:6<361::AID-CMR1>3.0.CO;2-L.

Kc, R. *et al.* (2010) 'New solenoidal microcoil NMR probe using zero-susceptibility wire', *Concepts in Magnetic Resonance Part B: Magnetic Resonance Engineering*, 37B(1), pp. 13–19. doi: 10.1002/cmr.b.20152.

Keifer, P. A. (1999) '90° pulse width calibrations: How to read a pulse width array', *Concepts in Magnetic*

Resonance, 11(3), pp. 165–180. doi: 10.1002/(SICI)1099-0534(1999)11:3<165::AID-CMR4>3.0.CO;2-D.

Lee, C. H. *et al.* (2015) 'Investigation of the subcellular architecture of L7 neurons of Aplysia californica using magnetic resonance microscopy (MRM) at 7.8 microns', *Scientific Reports*. Nature Publishing Group, 5(June), p. 11147. doi: 10.1038/srep11147.

Lee, C. H. *et al.* (2016) 'Magnetic Resonance Microscopy (MRM) of Single Mammalian Myofibers and Myonuclei', *Nature Publishing Group*. Nature Publishing Group, (January), pp. 1–9. doi: 10.1038/srep39496.

Littlejohn, G. R. *et al.* (2010) 'Perfluorodecalin enhances in vivo confocal microscopy resolution of Arabidopsis thaliana mesophyll', *New Phytologist*. Wiley Online Library, 186(4), pp. 1018–1025.

Minard, K. R. and Wind, R. A. (2001a) 'Solenoidal microcoil design. Part I: Optimizing RF homogeneity and coil dimensions', *Concepts in Magnetic Resonance*, 13(2), pp. 128–142. doi: 10.1002/1099-0534(2001)13:2<128::AID-CMR1002>3.0.CO;2-8.

Minard, K. R. and Wind, R. A. (2001b) 'Solenoidal microcoil design Part II: Optimizing winding parameters for maximum signal-to-noise performance', *Concepts in Magnetic Resonance*, 13(3), pp. 190–210. doi: 10.1002/cmr.1008.

Oerther, T. (2012) *Micro Imaging Manual for AV3 Systems*. Rev. 32. Rheinstetten, Germany: Bruker Biospin GmbH.

Olson, D. L. *et al.* (1995) 'High-Resolution Microcoil 1H-NMR for Mass-Limited, Nanoliter-Volume Samples', *Science*, 270(5244), pp. 1967–1970. doi: 10.1126/science.270.5244.1967.

Peck, T L, Magin, R. L. and Lauterbur, P. C. (1995) 'Design and analysis of microcoils for NMR microscopy.', *Journal of magnetic resonance. Series B*, pp. 114–124. doi: 10.1006/jmrb.1995.1112.

Peck, Timothy L., Magin, R. L. and Lauterbur, P. C. (1995) 'Design and Analysis of Microcoils for NMR Microscopy', *Journal of Magnetic Resonance, Series B*, pp. 114–124. doi: 10.1006/jmrb.1995.1112.

Radecki, G. *et al.* (2014) 'Functional magnetic resonance microscopy at single-cell resolution in Aplysia californica.', *Proceedings of the National Academy of Sciences of the United States of America*, 111(23), pp. 8667–72. doi: 10.1073/pnas.1403739111.

Tsai, W. T. (2011) 'Environmental property modelling of perfluorodecalin and its implications for environmental fate and hazards', *Aerosol and Air Quality Research*, 11(7), pp. 903–907. doi: 10.4209/aaqr.2010.12.0106.

Vegh, V. *et al.* (2012) 'High-field magnetic resonance imaging using solenoid radiofrequency coils.', *Magnetic resonance imaging*. Elsevier Inc., 30(8), pp. 1177–85. doi: 10.1016/j.mri.2012.04.027.

Vlaardingerbroek, M. T. and Boer, J. A. (2013) *Magnetic resonance imaging: theory and practice*. Springer Science & Business Media.

Webb, a G. (2013) 'Radiofrequency microcoils for magnetic resonance imaging and spectroscopy.', *Journal of magnetic resonance (San Diego, Calif. : 1997)*, 229, pp. 55–66. doi: 10.1016/j.jmr.2012.10.004.